# Local-field and effective-background effects in coupled integrated photonic waveguide systems

Anastasiia Sheveleva, Mathieu Leonardo, Christophe Finot, Pierre Colman

# Local Field and Effective background effects in coupled integrated photonic waveguides systems

Anastasiia Sheveleva[1], Mathieu Leonardo[1], Christophe Finot[1], and Pierre Colman *[1]

[1] *Laboratoire Interdisciplinaire Carnot de Bourgogne UMR CNRS 6303, Université Bourgogne–Franche-Comté, 9 Avenue Savary, 21000 Dijon, France**

(Dated: October 17, 2023)

The coupling constant between two nearby waveguides is usually predicted using formulas derived from the perturbative theory applied to the electromagnetic Maxwell's equations. These formulas however fail to provide any reliable estimate when the index contrast between the core of the waveguide and its cladding becomes large. We demonstrate in this paper that a good accuracy can be retrieved if the Local Field Effect is taken into account. Moreover, we show that in case of structured and inhomogeneous cladding, an Effective Background Index must be taken into account so that the Local Field Effect correction remains accurate. This theoretical study is the occasion for physics oriented discussions regarding the impact of the substrate on the inter-waveguides coupling constant.

Keywords: Coupled Waveguides, Integrated Photonics, Perturbative Methods in Electromagnetism, Local Field Effect, Effective permittivity

## I. INTRODUCTION

The fine control of the coupling strength between two nearby optical waveguides is a critical feature in photonics. Regarding applications, optical couplers are, for instance, an essential building block for photonic integrated chips [1–3]. If they can be considered as the simplest system of coupled waveguides, yet their thorough comprehension is a first essential step toward the control of much complex systems like nonlinear waveguide arrays [4–7], the realization of optical analogue to quantum effects [8–11], and topological systems [12–14]. Moreover mode coupling can also be invoked in order to explain mode dispersion [15] and can serve as a strategy for dispersion engineering [16, 17]. Consequently, this topic has been at the center of numerous theoretical and experimental investigations. These studies focused either on the effective parameters equations that can be used to describe coupled waveguides [18, 19], or on the link between the effective parameters and the waveguides geometry [20, 21].

A modern approach consists in describing the dynamics of waveguides arrays in terms of optical supermodes rather than individual waveguides. Because the supermodes are shaped by the inter-modes coupling constants, their chromatic dispersion will also be related to the latter. In particular, dispersion engineering through mode coupling has already been proved a successful strategy for double-ring resonators [22]. More recently, theoretical works proposed to combine this type of dispersion-engineering with the multimodal nature of waveguides arrays in order to facilitate the phase-matching during parametric processes [16, 17].These new applications require an acute knowledge of coupled waveguides systems, in particular regarding the chromatic dispersion of the coupling constants, and how the latter could be tuned. Moreover, technology has greatly evolved since the first theory about waveguides arrays: slab waveguides have been replaced gradually by more compact ridge waveguides which exhibit much higher optical confinement. As a result, current formulas developed according to perturbative models now fail when they are applied to these new nanophotonics systems. We will detail throughout this paper how these formulas fail; and how some simple modifications allow retrieving an acceptable accuracy.

## II. PERTURBATIVE ELECTROMAGNETIC METHOD IN GUIDED OPTICS

### A. Hamiltonian formulation of problems in perturbative photonics

Let us first recall the basis equations, and hypothesis, that lead to the coupling formula usually found in literature [18, 19, 23, 24].

$$\begin{aligned} \bigtriangledown \cdot \varepsilon_0 \varepsilon \boldsymbol{E} = 0 \quad \bigtriangledown \times \boldsymbol{E} = -\mu_0 \frac{\partial \boldsymbol{H}}{\partial t} \\ \bigtriangledown \cdot \mu_0 \boldsymbol{H} = 0 \quad \bigtriangledown \times \boldsymbol{H} = \varepsilon \varepsilon_0 \frac{\partial \boldsymbol{E}}{\partial t} \end{aligned} \tag{1}$$

We can first deduce from the translation invariance along the waveguide direction $\mathbf{x}$ that the optical mode can be decomposed as:

$$\begin{bmatrix} \boldsymbol{E}(x,y,z,t) \\ \boldsymbol{H}(x,y,z,t) \end{bmatrix} = \begin{bmatrix} \boldsymbol{E}(y,z) \\ \boldsymbol{H}(y,z) \end{bmatrix} e^{i\beta x - i\omega t} \tag{2}$$

Moreover, the longitudinal components of the field $\{E_x, H_x\}$ can be expressed from its transverse components $\{\boldsymbol{E}_\perp, \boldsymbol{H}_\perp\}$, so that the Maxwell's equations Eq.(1) can be expressed using only the latter. After some math, and following the guidelines in [25], we can define a generalized propagation equation where $|\psi\rangle =$

$[\boldsymbol{E}_\perp(y,z);\boldsymbol{H}_\perp(y,z)]$

$$\frac{\partial}{\partial x}\hat{B}\left|\psi\right\rangle = \imath\frac{\omega}{c}\hat{A}\left|\psi\right\rangle \tag{3}$$

The corresponding eigenvalue problem with value $\beta_0$ and eigenvector $|\psi_0\rangle = [\boldsymbol{E}_{\perp 0}(y,z);\boldsymbol{H}_{\perp 0}(y,z)]$ is then:

$$\beta_0\hat{B}\left|\psi_0\right\rangle = \frac{\omega}{c}\hat{A}\left|\psi_0\right\rangle \tag{4}$$

The hermitian operators $\hat{A}$ and $\hat{B}$ are

$$\hat{B} = \begin{bmatrix} 0 & -\vec{x}\times \\ \vec{x}\times & 0 \end{bmatrix}$$
$$\hat{A} = \begin{bmatrix} \sqrt{\frac{\varepsilon_0}{\mu_0}}\left[\varepsilon - \frac{c^2}{\omega^2}\bigtriangledown_t\times\left\{\vec{x}\cdot\left[\frac{1}{\mu}\vec{x}\cdot(\bigtriangledown_t\times)\right]\right\}\right] & 0 \\ 0 & \sqrt{\frac{\mu_0}{\varepsilon_0}}\left[\mu - \frac{c^2}{\omega^2}\bigtriangledown_t\times\left\{\vec{x}\cdot\left[\frac{1}{\varepsilon}\vec{x}\cdot(\bigtriangledown_t\times)\right]\right\}\right] \end{bmatrix} \tag{5}$$

Knowing an eigen-solution $|\psi_0\rangle$, the corresponding propagation constant $\beta_0$ is simply the Rayleigh quotient:

$$\beta_0 = \frac{\omega}{c}\frac{\langle\psi_0|\,\hat{A}\,|\psi_0\rangle}{\langle\psi_0|\,\hat{B}\,|\psi_0\rangle} \tag{6}$$

These equations are the starting point to construct a perturbative theory [24–26]. We now consider a system of coupled waveguides, where the second one is considered as a perturbation which modifies the field of the first (and vice versa), resulting in new optical modes $\left|\psi^{(t)}\right\rangle$. Using the Hamiltonian formulation developed previously we separate the parts corresponding to the isolated single waveguides equations $\hat{A}_0$ and its corrections $\Delta\hat{A}$:

$$\beta\hat{B}\left|\psi^{(t)}\right\rangle = \frac{\omega}{c}\left(\hat{A}_0 + \Delta\hat{A}\right)\left|\psi^{(t)}\right\rangle \tag{7}$$

By projecting Eq.(7) on the eigen modes of the isolated basis, the equation can be further simplified, namely by exploiting the hermitian property of $\hat{A}$ and $\hat{B}$. In this case the eigenvalue propagation equation becomes:

$$\left(\beta - \beta_0^{(i)}\right)\left\langle\psi_0^{(i)}\right|\hat{B}\left|\psi^{(t)}\right\rangle = \frac{\omega}{c}\left\langle\psi_0^{(i)}\right|\Delta\hat{A}^{(i)}\left|\psi^{(t)}\right\rangle \tag{8}$$

The index $i = \{1,2\}$ indicates whether the first or second isolated waveguide is considered. Following the conventional coupled-mode theory [3, 18] the eigenmode supported by the waveguides array (with the respective propagation constant $\beta$) is then approximated as a combination of the isolated waveguides' modes, hence:

$$\left|\Psi^{(t)}\right\rangle = \left(a_1\left|\psi^{(1)}\right\rangle + a_2\left|\psi^{(2)}\right\rangle\right)e^{i\beta x} \tag{9}$$

After substituting $\left|\Psi^{(t)}\right\rangle$ to Eq.(8) and rearranging the terms we obtain the two-unknown set of equations:

$$B^{-1}\begin{bmatrix}\beta-\beta_0^{(1)} & 0\\ 0 & \beta-\beta_0^{(2)}\end{bmatrix}B\begin{bmatrix}a_1\\a_2\end{bmatrix} = \frac{\omega}{c}B^{-1}\Delta A\begin{bmatrix}a_1\\a_2\end{bmatrix} \tag{10}$$

where $\Delta A, B$ are matrices with elements expressed as:

$$B_{ij} = \iint_S \boldsymbol{x}\cdot(\boldsymbol{E}^{(i)*}\times\boldsymbol{H}^{(j)} - \boldsymbol{H}^{(i)*}\times\boldsymbol{E}^{(j)}) \tag{11}$$

$$\Delta A_{ij} = \sqrt{\frac{\varepsilon_0}{\mu_0}}\iint_S\left[E_x^{(i)*}E_x^{(j)}\frac{\varepsilon_i\Delta\varepsilon_i}{\varepsilon_t} + D_y^{(i)*}D_y^{(j)}\frac{\Delta\varepsilon_i}{\varepsilon_i\varepsilon}_j + E_z^{(i)*}E_z^{(j)}\Delta\varepsilon_i\right] \tag{12}$$

Here $\boldsymbol{E}(y,z)^{(i)}$ is the eigen-field of the $i^{th}$ waveguide, and $\varepsilon_i$ its dielectric constant. Correspondingly $\Delta\boldsymbol{\varepsilon}_i$ is a perturbation introduced to the $i^{th}$ waveguide by the other one; $\boldsymbol{\varepsilon}_t = \boldsymbol{\varepsilon}_i + \Delta\boldsymbol{\varepsilon}_i$ is then the total dielectric portrait of the system, varying in the transverse $(y,z)$ plane. If we assume $\beta_0^{(1)} = \beta_0 + \frac{\Delta\beta}{2}$ and $\beta_0^{(2)} = \beta_0 - \frac{\Delta\beta}{2}$, then Eq.(10) turns into:

$$(\beta-\beta_0)\begin{bmatrix}a_1\\a_2\end{bmatrix} = B^{-1}\left(\frac{\Delta\beta}{2}\begin{bmatrix}-1&0\\0&1\end{bmatrix}B + \frac{\omega}{c}\Delta A\right)\begin{bmatrix}a_1\\a_2\end{bmatrix} \tag{13}$$

For identical waveguides $\Delta\beta = 0$, Eq.(13) can be further simplified as:

$$(\beta-\beta_0)\begin{bmatrix}a_1\\a_2\end{bmatrix} = \frac{\omega}{c}B^{-1}\Delta A\begin{bmatrix}a_1\\a_2\end{bmatrix} \tag{14}$$

The case of different waveguides, namely how the mismatch between the waveguides impacts their effective coupling [27, 28], will be discussed further in another article. The $\{i,j\}$ off-diagonal elements correspond to the coupling $\kappa_{ij}$ between the $i^{th}$ and the $j^{th}$ waveguides. Note that the propagation equation is constructed such that the flux of the Poynting vector (hence $\langle\Psi|\,\hat{B}\,|\Psi\rangle$) is preserved throughout propagation. If applied to the case of moderate modifications of an isolated waveguide, Eq.(8) produces a good quantitative estimate. It can

cope in particular with moving boundaries and polarization issues in high index problems [24, 26]. More details regarding the underlying mathematics and the corresponding electromagnetic Hamiltonian formulation of such theory can be found in [24].

The coupling between two adjacent waveguides is ascribed to the evanescent tail of the optical mode which extends far away from the core region of the waveguide and interacts with the neighboring waveguides. For negligibly overlapping waveguides modes ($B_{ij} = \delta_{ij}$) [19], and neglecting both the longitudinal component of the electric field ($E_x = 0$) and the polarization effects caused by the dielectric interface, Eq.(14) admits a simple analytical form, that is [29]:

$$\kappa_{ij} = \frac{\omega\varepsilon_0 \iint_S \Delta\boldsymbol{\varepsilon}_i \boldsymbol{E}^{(i)*} \cdot \boldsymbol{E}^{(j)}}{\iint_S \boldsymbol{x} \cdot (\boldsymbol{E}^{(i)*} \times \boldsymbol{H}^{(j)} - \boldsymbol{H}^{(i)*} \times \boldsymbol{E}^{(j)})} \qquad (15)$$

Equation 15 is identical to the formulation derived in seminal works [19, 23, 29]. The relative impacts of the polarization of the electromagnetic field, including the impact of the longitudinal $\boldsymbol{E}_x$ component [24, 30], or the non-orthogonality of the isolated waveguide basis [19, 23] (hence $B_{ij} \neq 0$ for $i \neq j$) result in about minor changes (for a proper comparison please refer to Appendix A). Therefore for sake of clarity, only one of these curves will be for the figures, and simply labeled as "previous works". As seen in Fig.A1, Eq.(15), or any other similar derivations, actually fails to provide an accurate estimate of the coupling constant (for the high index contrast systems, as the ones considered in this paper).

### B. Coupled waveguide configuration

In order to help the discussion, and provide quantitative information regarding the accuracy of perturbative theory applied to systems of coupled waveguides, we investigate in this article two types of systems that may represent typical situations found in integrated photonics.

First we consider a silicon on insulator coupler [31] composed of two 220 nm-high and 803 nm-wide waveguides (Fig.1-(a)). This geometry can be considered as a standard in current integrated photonics industry. It exhibits one of the largest confinement between the core of the waveguide and its cladding. As such, nearly all the light remains confined within the core of the waveguide, and the evanescent tail decays very sharply. This system presents one of the largest index contrast in dielectric photonics.

The second system under investigation is composed of two silicon-nitride ($SiN$) rib waveguides [32, 33] that are partially etched, leaving out a 260 nm silicon-nitride membrane on insulator (Fig.1-(b)). The index contrast provided by $SiN$ ($n = 1.6$ up to 2.2) is quite similar to what is found for emerging material like $TiO_2$ ($n = 2.5$) [34, 35] and $Ta_2O_5$ [36]. To provide indicative numbers, the contrast between the core of the waveguide and its silica substrate is about $\Delta\varepsilon = 2.4$, hence nearly 50% smaller than the contrast with the air cladding $\Delta\varepsilon = 3.5$. Moreover, the presence of a high-index thin $SiN$ layer on top of the silica substrate helps extending the evanescent tail of the optical mode farther away from the waveguide. Therefore, despite the index contrast being formally large $\Delta\varepsilon > 1$, the optical mode is actually weakly confined in the core of the waveguide, like this is the case for low contrast systems. Furthermore, we can also expect that the properties of this system also depend strongly on the exact structure of the air-SiN-Silica stack. This study is thus the occasion to explore the fundamental differences between fully etched and rib-waveguides. These systems would constitute a good benchmark to test the robustness and accuracy of perturbative theory in photonics.

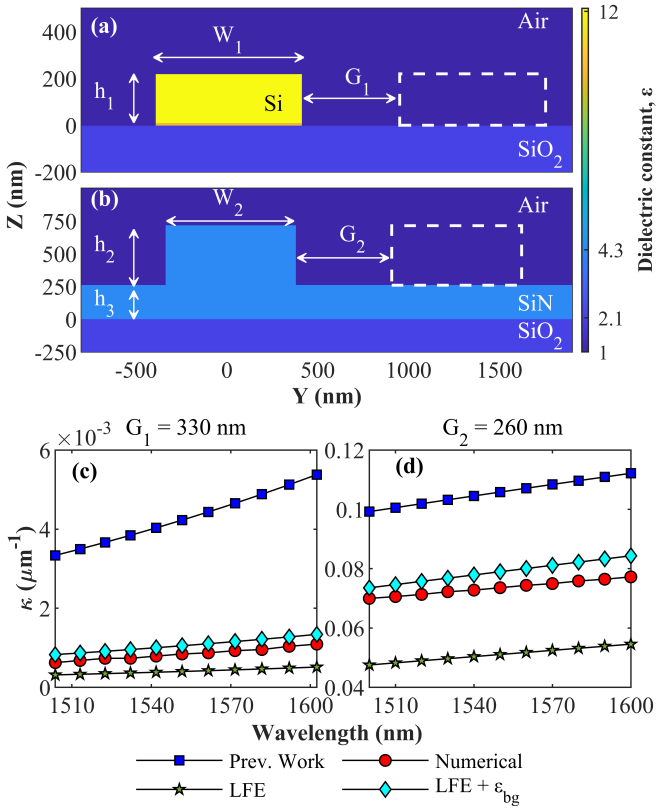


FIG. 1. . (a) Dielectric map of the silicon ridge waveguide considered in this work. ($W_1 = 803$ nm , $h_1 = 220$ nm). (b) Dielectric map of the silicon-nitride rib-waveguide ($W_2 = 715$ nm , $h_2 = 455$ nm , $h_3 = 260$ nm). (c) Coupling constant $\kappa$ for two silicon waveguides separated by $G_1 = 330$ nm, as a function of the wavelength. Squares: previous works [18, 19, 23, 24]. Red circles: Numerical simulation [37]. Green stars: theory including the Local Field Effect (LFE). Cyan diamonds: Theory including the LFE complemented by the concept of the effective background ($\varepsilon_{\rm bg}$). (d) Same as (c), but for the SiN rib waveguides, considering an inter-waveguide spacing of $G_2 = 260$ nm.

In this article the results of Eq.(14) and Eq.(15) are

compared against direct simulation of the coupled waveguide system. The electromagnetic field distribution of the isolated waveguides is obtained by simulation using the same plane wave expansion simulation method, namely the MIT Photonics Band package (MPB) [37]. Waveguides' widths and separations are chosen to match precisely the discretisation grid, as to minimize smoothing errors. Exact parameters used for the MPB simulations, and the relative accuracy of the numerical computation, are presented in Appendix B. Since the chromatic dispersion is mostly dominated in nanophotonics waveguides by the geometry, dispersionless material is assumed.

## III. LOCAL FIELD EFFECT

We ascribe the discrepancy in Fig.1-(c,d) between the numerical simulations and the result of Eq.(11) to the fact that the first order corrective theory assumes no modifications in the nominal mode field distribution, despite the introduction of a dielectric perturbation. For large index contrast systems (hence $\Delta\varepsilon > 1$), this assumption however does not hold because the resulting dipole $\Delta\varepsilon_i \boldsymbol{E}^{(i)}$ created by the dielectric perturbation would then become much larger than the nominal electric field $\boldsymbol{E}^{(i)}$ itself. Therefore the correction must not be considered as perturbative. Under the influence of the dielectric perturbation $\Delta\varepsilon(r)$, the nominal electric field $\boldsymbol{E}_0$ of an optical mode is modified [38, 39]:

$$\boldsymbol{E} = \boldsymbol{E}_0 + \iint_{\boldsymbol{r}\neq\boldsymbol{r}'} \left(\overleftrightarrow{\boldsymbol{G}}_0(\boldsymbol{r},\boldsymbol{r}')k_0^2\Delta\varepsilon(\boldsymbol{r}')\boldsymbol{E}(\boldsymbol{r}')d\boldsymbol{r}'\right) - \frac{L\Delta\varepsilon}{\varepsilon_{\mathrm{bg}}}\boldsymbol{E} \tag{16}$$

$\overleftrightarrow{\boldsymbol{G}}_0$ is the Green function (GF) of the unperturbed system [38], and $\boldsymbol{E_0}$ the unperturbed optical mode. The second term in the right hand side of Eq.(16) is the well-known contribution of the Green function. The convolution has two major consequences. Firstly, it impacts the electromagnetic fields distribution even outside the region where the dielectric permittivity is modified. Secondly, the convolution can result in multiple scattering: the resulting optical field does not then solely depend on the dielectric perturbation, but also on the presence of nearby dielectric interfaces. The specificity of the problem considered here is that the optical field propagates in the **x** direction with a phasor factor (i.e. $n_{eff}$) that is greater than the nominal dielectric permittivity of the cladding. Consequently the Green function is of evanescent nature, hence tightly localized. As a rule of thumb, the decay rate of the GF is of the order of $\alpha = 2\pi/\lambda\sqrt{n_{eff}^2 - \varepsilon}$; which results into $\alpha = 9.7\ \mu m^{-1}$ and $\alpha = 6.2\ \mu m^{-1}$ for the silicon and the silicon nitride waveguides, respectively. Comparing $\alpha^{-1}$ to the characteristic waveguides' widths $W$ and inter-waveguide separations G, we can infer that multiple scattering will be a second order correction in Eq.(16). Therefore, except in the close vicinity of the interface of the dielectric perturbation, the resulting changes in the electric field $\boldsymbol{\Delta E} = \boldsymbol{E} - \boldsymbol{E}_0$ are to a good approximation somewhat proportional to the local averaging of $\boldsymbol{E}$.

The third term in Eq.(16) is called the Local Field Effect. The origin of the LFE is deeply rooted to the divergence of the Green function in the source region: at this specific location the order of the convolution and of the curl operators cannot be interchanged [40]. When the dielectric background ($\varepsilon_{\mathrm{bg}}$) differs from vacuum, it is indeed proved that a correct mathematical derivation results in the correction of the defect polarization $\delta\varepsilon(\vec{r})$ by a dyadic factor $L\Delta\varepsilon\vec{E}(\vec{r})/\varepsilon_{\mathrm{bg}}$ ($L = 1/3$) [40–42]. As we will discuss it in more details later, the $L$ factor depends on the geometry of the problem, namely the shape of the principal volume, hence the symmetry of the discretization grid. For a general problem computed on a square grid: $L = 1/3$. For other problems, the value of $L$ may change. In the absence of multiple scattering, and for small scale perturbations, the LFE contribution dominates. For an homogeneous perturbation over a zone where the electric field varies slowly, a formulation very similar to the LFE can also be derived [41]. The resulting electromagnetic field can then be reasonably approximated as [39]:

$$\boldsymbol{E} = \frac{\boldsymbol{E}_0}{1 + \frac{L\Delta\varepsilon}{\varepsilon_{\mathrm{bg}}}} \tag{17}$$

$\varepsilon_{\mathrm{bg}}$ is the background permittivity at the source point. The initial defect polarizability is screened, resulting in a final formula close to the Clausius-Mossotti's one [43–45]. However the physical origins greatly differ. In the case of the Clausisus-Mossotti theory, the reduced apparent polarizability comes from the screening effect that originates from the neighboring dipoles that form an homogeneous polarizable background which counters the initial perturbation. For the LFE, it can be interpreted as the feedback action of a single and isolated dipole on itself, more akin an impedance mismatch for an antenna: only a small fraction of the polarization defect actually contributes to the modification of the electric field. Even though the resulting effects have similar formulations, and therefore they can be all included in the same formula, LFE and screening effects must still be considered as distinct phenomena. Note that the screening action of Eq.(17) would also apply to estimate the defect polarization induced by a dielectric perturbation, which is then not simply $\Delta\varepsilon E_0$ anymore.

The inclusion of the LFE in Eq.(2), is shown in green-stars line in Fig.1-(c,d). In brief, the coupled waveguide problem is determined in Eq.(10)-(14) following the Petrov-Galerkin approach that consists in reducing the dimensionality of the problem by using carefully selected test-functions. In particular the hermiticity of $\hat{A}$ simplifies greatly the resulting problem through the choice of $\left\langle \psi_0^{(i)} \right|$ as test-functions basis. This extreme simplifica-

tion comes at the cost of accuracy. Some precision can then be retrieved through a different choice of the solution functions basis : here Eq.(17) is then injected into Eq.(9). We see that it improves notably the accuracy regarding the silicon waveguide (Fig.1-(c)). The results are more mitigated for the silicon nitride waveguide on a $SiN/SiO_2$ substrate (Fig.1-(d)). The silicon waveguides have the highest index contrast, so that the first order perturbative theory fails more than for SiN. But in turn the changes in the electric field distribution are much simpler, without long range contribution of the Green Function; and consequently they can be better approximated using the simple formula in Eq.(17).

## IV. HIGH CONTRAST INTEGRATED-PHOTONICS

Corrective models of the first order consider small changes to the initial problem. Regarding photonic systems, this implies that the changes $\Delta\varepsilon$ to the nominal dielectric distribution are small enough so that the corresponding defect dipole $\Delta\varepsilon\boldsymbol{E}$ remains much smaller than the nominal optical field $\boldsymbol{E}$. Indeed any modification of a dielectric interface results in the creation of unphysical free charges if one assumes that the electric field distribution remains unchanged. This issue is as severe as the index contrast is large. As illustration, two typical examples are presented and discussed in thorough details in section II B, Fig.1-(c,d). This typical problem is not surprising, and it can be tracked back to the issue related to the use of an incomplete basis when performing a type of Resonant State Expansion (RSE) [24, 26, 46]. Indeed the perturbative and standard modes expansion methods usually assume that it is possible to describe the modified systems using only the solutions of the unmodified one. However, these few modes are not enough to enforce the divergence free of the electric field in presence of the large index contrast dielectric perturbation (namely the presence of the second waveguide for a coupled waveguides system).

Several strategies can be employed to solve this issue. First, it can be solved by completing the ersatz modes basis with a few "unphysical" modes that are pure mathematical non-divergence-free solutions of the Helmholtz's equation [47, 48]. Albeit this technique results in a better numerical accuracy, it does not provide much insight about the actual physics governing the coupled integrated waveguides systems. Another approach would rely on Quasi-Normal Modes (QNMs) [49, 50]. For resonant (open) systems, QNMs expansion proves to be quite powerful providing enough modes are accounted for. Hopefully these systems are mostly governed by the resonances with the highest quality factor so only a few QNMs, which can be easily identified, are sufficient [51]. For non-resonant systems such as waveguides the choice of the right QNMs might not be however straightforward. The possibility offered by this technique will still be investigated and discussed in later study. Finally the coupling constants could also be retrieved following the analysis of brute force computations of the full system of coupled waveguides [52]. This is usually a simple task on modern computers, but it lacks then any insight regarding the physics governing coupled waveguides systems, hence no generalization could be made.The main disadvantage of all these strategies is that they require specific knowledge of the final system, hence the final properties cannot be simply inferred *a priori*. Besides, the large number of modes involved for these accurate modeling complicates the description of the system, hence its design.

The standpoint we chose in this paper is to investigate the first order models used thus far for describing coupled waveguides systems [19, 23]. Indeed, the great advantage of the formulations developed in this context is that they remain simple. All the properties are derived from analytical integral formula that only require the prior knowledge of general properties of the isolated waveguides. And therefore a large variety of configuration can then be tested without requiring additional nor complex computations. The objective is to extend the current theories past its first order approximation, in order to improve its accuracy, while preserving their intrinsic simplicity.
The solution we developed here consists in modifying the nominal optical modes so that the mode expansion becomes more accurate, while keeping the required number of modes minimal. This could be achieved by the inclusion of the Local Field Effect (LFE) [40–42] complemented by an effective background theory (Fig.1-(c,d)). We rely in particular on the developments that have been recently made regarding disorder in photonics (small perturbations, but high-index contrast) [42, 53, 54], and demonstrate that they can be extended then to the general case.

## V. LFE ON EFFECTIVE BACKGROUND

For better comparison with previous theories, we consider in this article that the individual waveguides only support one single mode, whereas higher order modes with different polarization actually do exist in integrated waveguides. These restrictions impact the accuracy of the results which we present here; but we believe it allows for a fairer comparison, and also clearer subsequent physics oriented discussions. Based on the results presented in Fig.1, taking the LFE into account improves notably the results, but some discrepancies still remain, mostly visible for the silicon nitride waveguides. The remaining error could be partly attributed to an inadequate choice of $\varepsilon_{\text{air}}$, resulting in an over-estimation of the impact of the LFE. Indeed the seminal theory of the LFE considers only the case of homogeneous dielectric backgrounds; and in the situation where the perturbation occurs at a dielectric interface, the correct value of the background permittivity is uncertain [42]. Here,

while the second waveguide occupies a zone previously filled with air only (hence $\varepsilon_{\rm air} = 1$), it is still only a few hundreds of nanometers away from a higher index ($\varepsilon_{\rm SiN} = 4.4$, $\varepsilon_{\rm SiO2} = 2.3$) substrate. Therefore it can be expected that the presence of a high index dielectric interface in the near field of the source region has an impact on its radiation properties [55, 56]. Indeed we checked that, for the case of a waveguide immersed in an homogenous background, the LFE correction results into a more reliable estimation of the coupling constant (Fig.C1). Note that for the silicon waveguides, the index contrasts between the waveguide's core and either the Silica substrate or the air cladding are - comparatively - about the same, so that the exact value taken for background permittivity has a lesser influence on the final result.

In its seminal derivation, the LFE is computed for an isolated dielectric perturbation in an infinite and homogeneous background. The dielectric permittivity $\varepsilon_{\rm bg}$ stated in the LFE effect is intrinsically linked to the Green function, which is simply related to the homogeneous medium's permittivity. The main difficulty in a practical situation is to adapt the LFE when the presence of either a dielectric inhomogeneity or a structuration notably alters the features of the Green function [57]; hence the effective value of $L\varepsilon_{\rm bg}$ [58]. Considering that the LFE depends on both the local geometry of the problem (for the L value) and the dielectric contrast, this effect can be generalized to the concept of defect polarizability [42] where its impact can be calibrated for a given class of defect. In brief, it consists in fitting the prefactor that would correct the first order perturbative theory versus the dielectric change $\Delta\varepsilon$, for a given class of problems. The resulting calibration function holds some universality and can be then re-used for other perturbative problems of the same class, hence without requiring complementary ab-initio simulations. Indeed the impact of both the geometry, namely the value of L, and the dielectric structuration, namely $\varepsilon_{\rm bg}$, are then intrinsically accounted for. This approach has been successfully applied to the investigation of the impact of random imperfections in high index contrast micro-photonics systems such as photonic crystals [42, 59]. We demonstrate here that this approach, which has been first developed for small perturbations, remains valid even in the case of an extended perturbation (i.e. waveguides). Furthermore, we focus the discussion on the impact of the local dielectric structuration, and show that it has a major impact on the inter-waveguide coupling; and that the correct LFE factor can be estimated quite simply [60].

Considering that electromagnetic problems are solved numerically over a finite grid, and that dielectric perturbations are themselves of finite size, the numerical solution of Eq.(16) in the limit of an ultra-small volume around the source region $\delta_V \to 0$ provides actually the correct solution for the local self-screened response for a dielectric perturbation, including the LFE and other GF induced scattering [61, 62]. At this point, both the LFE and the local screening effect cannot be distinguished anymore from each other[41]. In order to get a better understanding of the role of the substrate, we therefore solved the Green Function response to a dielectric perturbation $\Delta\varepsilon$. For generality we consider an **{x,y}** invariant medium where there exists along **z** an air-dielectric interface, namely a single air-Silica interface for the case of the silicon waveguides, and an air/silicon-nitride/silica interface for the case of the silicon-nitride waveguides. Considering Eq.(2) that the electromagnetic field propagates with an effective propagation phasor along **x** $\beta = \frac{\omega}{c} n_{eff}$ the equation to solve is:

$$\bigtriangledown \times \bigtriangledown \times \overleftrightarrow{\boldsymbol{G}}_0 + 2\imath\frac{\omega}{c} n_{eff}\vec{x} \times (\bigtriangledown \times \overleftrightarrow{\boldsymbol{G}}_0) + \left(\frac{\omega}{c}\right)^2 n_{eff}^2 \vec{x} \cdot (\vec{x}.\overleftrightarrow{\boldsymbol{G}}_0) + \left(\frac{\omega}{c}\right)^2 (\epsilon(y,z) - n_{eff}^2)\overleftrightarrow{\boldsymbol{G}}_0 = \overleftrightarrow{\delta}(y - y_0, z - z_0) \quad (18)$$

The important point about the problem considered here is that $(\varepsilon(y,z) - n_{eff}^2) < 0$ at the position of the perturbation. Therefore GF solution of Eq.(18) is not a propagating wave but an evanescent-decaying, hence tightly localized, function. This behaviour limits strongly multiple-scattering. It also strongly alleviates the problems related to the finite size of the simulation domain. We solved Eq.(18) using the Fourier modal expansion (grid size of 10 nm) assuming an unperturbed uniform electric field purely **y**-polarized $\boldsymbol{E}_0 = 1\vec{y}$. Indeed the mode field distributions of the waveguides modes considered here are **y**-polarized to about 90%. Thus these simplifications are still retaining the important features of the initial problem, while allowing a simpler discussion and computation [61, 62]. The result for the case of the silicon waveguide is shown in Fig.2(a,d).

In contrast to the approximation of the first order perturbation theory which assumes no modifications in the electric field (Fig.2(c,f)), the new displacement field $D_y$ that is obtained by changing the mode basis in Eq.(9) is now divergence-free, as seen in (Fig.2(h)). A strong modification ($\Delta\varepsilon > 1$) results in Fig.2(a) into a corresponding decrease of the total electric field in order to minimize discontinuity of the displacement field. This retro-action effect is therefore as severe as $\Delta\varepsilon$ is large. Looking into more details, we observe that the residual discontinuity is compensated by a gradient located at the edges of the dieletric perturbation. The restriction of the changes of the electric field to a generalized LFE cannot take into account these gradients. The LFE complemented by the concept of effective background appears in Fig.2(b,e) as a crude approximation of the exact field.

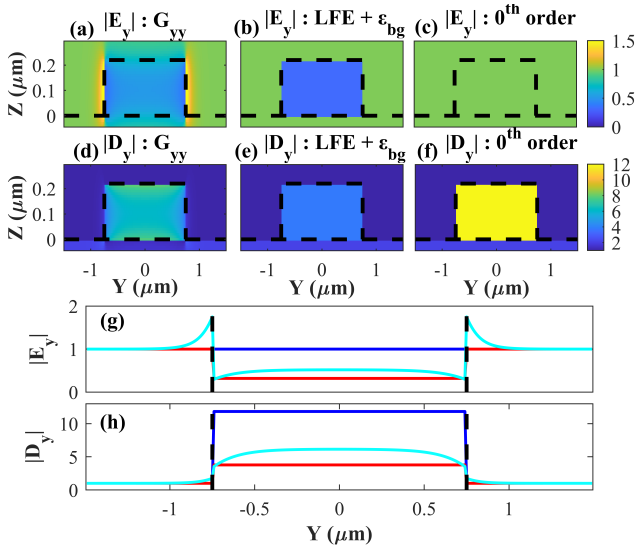


FIG. 2. Case of silicon waveguides. (a-c) y-component of the Electric Field resulting from the perturbation of an initial homogeneous $\boldsymbol{E} = 1\boldsymbol{y}$ field by a dielectric perturbation $\Delta\varepsilon$ which corresponds to the presence of the second waveguide. (a) is the solution of Eq.(16) restricted to the y-component of the field. (b) the result of the Local Field Effect assuming an effective background $\varepsilon_{\text{bg}} = 1.7$. (c) Initial Coupled mode formulation where no changes of the Electric field are assumed (i.e. $0^{th}$ order theory). Black-dashed lines indicate the position of the dielectric perturbation and the limit between the air-cladding and the underneath silica substrate. (d-f) y-component of the displacement field. (g-h) Variation of the electric Field (resp. Displacement Field) along y, for an altitude of 110 nm (Half the waveguide's height). Dark blue: zeroth order theory (no changes in the nominal electric field). Red: LFE theory assuming an effective background. Light Blue: Solution of Eq.(18).

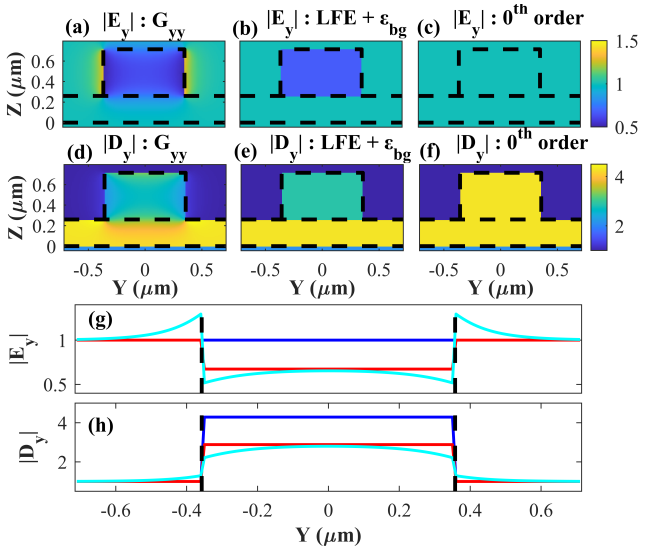


FIG. 3. Case of silicon nitride waveguides. (a-c) y-component of the Electric Field resulting from the perturbation of an initial homogeneous $\boldsymbol{E} = 1\boldsymbol{y}$ field by a dielectric perturbation $\Delta\varepsilon$ which corresponds to the presence of the second waveguide. (a) is the solution of Eq.(16) restricted to the y-component of the field. (b) the result of the Local Field Effect assuming an effective background $\varepsilon_{\text{bg}} = 2.7$. (c) Initial Coupled mode formulation where no changes of the Electric field are assumed (i.e. $0^{th}$ order theory). Black-dashed lines indicate the position of the dielectric perturbation and the limit between the air-cladding and the underneath substrate, which is composed of a thin 260 nm SiN layer on top of a Silica substrate. (d-f) y-component of the displacement field. (g-h) Variation of the electric Field (resp. Displacement Field) along y, for an altitude of 230 nm (Half the waveguide's height). Dark blue: zeroth order theory (no changes in the nominal electric field). Red: LFE theory assuming an effective background. Light Blue: Solution of Eq.(18).

Note that the accuracy of the LFE approximation might be directly related to the evanescent nature of the perturbation problem outside the waveguide's core region: multi-scattering can be neglected providing the waveguides are not too close from each other. Regarding the silicon-nitride waveguides, the corresponding comparison is shown in Fig.3.

Whereas solving Eq.(16) assuming a purely **y**-polarized field worked well for the silicon case, this approximation is a bit worse for the SiN configuration. Its accuracy actually directly depends on the strength of the longitudinal electric field [30]. It illustrates the complexity introduced by the structured substrate, namely the presence of a thin SiN layer, compared to a cladding of low refractive index.

The critical approximation that is made about the evaluation of Eq.(16) is the absence of standing waves between the dielectric perturbation and the initial waveguide [18]. The conclusions we draw out are then very general: it involves only the structure of the substrate; but disregards subtle effects that would occur at precise inter-waveguides separations. In particular, this approximation does not hold for ultra small gap separations where the system becomes then a slotted photonic structure which localizes a large portion of its electric field precisely inside the gap. Regarding the subsequent derivation of the LFE (Eq.(17)), the main simplification resides in the absence of a field gradient close to the dielectric interface. That said, the resulting improvement can still be clearly observed in Fig.1.

## VI. EFFECTIVE BACKGROUND

As a result, the key point of the LFE concerns the evaluation of the effective background permittivity $\varepsilon_{\text{bg}}$. The value of $\varepsilon_{\text{bg}}$ in Eq.(17) can be chosen as the fitting parameter that matches best the result of Eq.(16). It only depends on the dielectric configuration of the cladding/substrate. Thus it can be calibrated for a given technology. Note that for an uniform dielectric cladding, then $\varepsilon_{\text{bg}}$ is simply the latter permittivity, as stated by the nominal LFE derivation (this is illustrated further

in Fig.C1). Same-wise, the value of $\varepsilon_{\rm bg}$ does not depend on the size of the dielectric perturbation; the gradient features set aside. Interestingly, this value can actually be well approximated as the average permittivity felt by the optical mode away from the waveguide's core: $\varepsilon_{\rm bg} = \int \varepsilon(r)|\boldsymbol{E}|^2 / \int |\boldsymbol{E}|^2$. Consequently, if the concept of the effective background permittivity can appear so far as a mathematical fitting parameter, we demonstrate next that it is uniquely defined, and that it is deeply rooted to the optical mode features.

Indeed, let consider how the coupling constant evolves with increasing inter-waveguide spacing. It evolves similarly as the evanescent tail of the optical mode decays away from the waveguide. Therefore, if the mode propagates according to the effective index $n_{\rm eff}$, then the coupling constant must decay with a rate $\alpha = k_0\sqrt{n_{\rm eff}^2 - \varepsilon_{\rm bg}}$ where $k_0$ is the vacuum wave-vector. Thus, knowing the coupling constant for one inter-waveguide spacing, its values at other separations distances can be easily extrapolated.

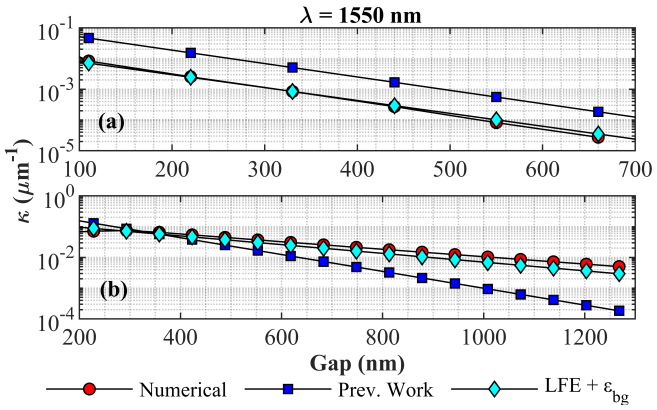


FIG. 4. (a-b) Evolution of the coupling constant $\kappa$ as function of the inter-waveguide spacing (Gap). The results obtained from perturbation theories for a Gap of 300 nm are assumed to vary with a decay rate $\alpha = k_0\sqrt{n_{\rm eff}^2 - \varepsilon_{\rm bg}}$. Red circles: results from direct simulations. Blue squares: previous perturbative theory where $\varepsilon_{\rm bg}$ is assumed to be equal to the cladding permittivity, namely $\varepsilon_{\rm bg} = \varepsilon_{\rm air} = 1$. Cyan diamonds: New formulation considering an effective background. (a) Case of silicon waveguides, $\varepsilon_{\rm bg} = 1.7$. (b) Case of silicon nitride waveguides, $\varepsilon_{\rm bg} = 2.7$

We see that assuming the nominal vacuum's permittivity ($\varepsilon_{\rm bg} = 1$, blue squares in Fig.4-(b)) results in a large overestimation of the decay rate. This is no surprise because the optical mode decays both in the cladding and in the substrate; and energy can be exchanged between these two media. As a result the actual decay rate is somehow a mixture of the cladding's and the substrate's ones. However, if one considers now the effective permittivity as the one just defined previously ($\varepsilon_{\rm bg} = 2.7$, cyan diamonds in Fig.4-(b)), the nominal decay factor now matches the numerical simulation. Regarding the silicon ridge waveguide (Fig.4-(a)), the effective index is much larger than the background permittivity so that small changes in the value of $\varepsilon_{\rm bg}$ have a much lesser impact than for SiN - and lower indices - waveguides.

From this analysis, we can conclude that the effective background that we introduced is both involved in the LFE and in the natural decay of the optical mode away from the waveguide's core. This is actually no surprise that the optical mode and its associated Green Function share some properties. Indeed according to the Kirchhoff theory, the decaying tail of the optical mode can be interpreted as the propagation -hence controlled by the Green Function- of light from the waveguide's core, which serves as source. The value of $\varepsilon_{\rm bg}$ is then uniquely defined; and therefore must also be considered as a fundamental property of the optical mode, like for instance its effective index $n_{eff}$.

If the complex numerical developments made in section V are essential in order to demonstrate formally that the concept of effective background permittivity is fully justified, hence is not an arbitrary and convenient fitting parameters, we would like to insist on the fact that reliable estimate of $\varepsilon_{\rm bg}$ can be accessed by looking simply at the field decay of the optical mode. In this prospect, even though the coupling for one specific inter-waveguide spacing can be estimated more accurately using direct simulation than the current analytical approach, we believe it is also equally important to have a reliable model to extrapolate the coupling at different spacing, hence being aware that $\varepsilon_{\rm bg}$ might not equals the nominal cladding index. This is in particular essential for large waveguides separations where the coupling may be too small for being computed accurately, and therefore is often extrapolated from values measured at smaller separations.

## VII. LIMITS AND PERSPECTIVES OF THE PERTURBATIVE APPROACH FOR COUPLED WAVEGUIDES

Compared to the models used previously, the Local Field Effect, complemented by the concept of effective background, improves the estimation of the coupling constant by nearly an order of magnitude. That said, as seen in Fig.1-(c,d), some errors still remain. If usually the discrepancy is blamed indistinctively on the high index contrast, we can be a bit more specific here. Note that the specificity of the SiN waveguides systems comes from its index contrast which is of intermediate value. Indeed the index contrast is strong enough ($\Delta\varepsilon = 3.29$) to result in a strong confinement, but it is still weak enough so that the exponential tail extends over a very long range ($k_0\sqrt{n_{\rm eff}^2 - \varepsilon_{\rm bg}} = 3.4\ \mu m^{-1}$). This sensibility would make SiN a platform of choice for coupled waveguides and sensing applications. However the final properties of this type of system are then much harder to infer using simple analytical formula.

Regarding the rib and ridges waveguides investigated in this paper, the main source of errors for previous analytical formulations clearly comes from the local field

effect, which was never considered. Next comes the definition of the effective background, which helps further to improve the accuracy in case of complex substrate/cladding. Other limitations may mainly come from the presence of higher order modes. For the sake of simplicity, and to allow a fairer comparison with previous works, the waveguides are supposed here to possess only a single guided mode. Actually, integrated waveguides support higher order modes, and modes of different polarization. These modes are orthogonal by construction but the presence of a second waveguide, acting as a perturbation, can couple them. This effect is as strong as the modes have a similar propagation constant, so it has a great impact on systems with either rotational symmetry (polarization degeneracy), or very large waveguide (small inter-mode spacing). In principle, Eq.(9) and Eq.(8) can be extended to include the impact of other modes. Note that the presence of angled dielectric interfaces results into further mixing between TE and TM polarized modes. Our choice of square waveguides with high form factor minimizes the impact of other modes and polarization effects, so that the LFE is singled-out. In the most general case, the relative impact of the LFE might be partly screened by multimodal and polarization effects.

In any case, the LFE is always present. Eventually its magnitude may vary depending on the local geometry, as it has been demonstrated previously [42]. Its magnitude is directly related to the ratio between the index contrast and the initial permittivity at the position of the perturbation, according to Eq.(17). Consequently, a change of the permittivity by $\Delta\varepsilon \approx 0.3\varepsilon_{\mathrm{bg}}$ would result into a correction of the coupling coefficient by about 10%. Considering the others effects at play in coupled waveguide systems (higher order modes, polarization, multi-scattering properties of the GF, etc.), this could be considered as about the limit where LFE must be taken into account. An important point is that the LFE is dissymmetric depending if the perturbation consists in a dielectric addition on a low index background, or a dielectric subtraction on a high index material. Conversely, we see that the modification of the core of a waveguide would have a reduced LFE contribution, compared to a modification of its cladding. When it comes to ultra-small waveguides separations, or the design of slotted waveguides, the right strategy would be then to consider a large initial waveguide whose center has been etched, rather than to use the two-coupled-waveguide description. As practical design rules, especially regarding perturbative - or even mode expansion- theories, the key point is to start with the initial structure which is the closest to the final one.

If the present article focuses on the Local Field Effect, the approach we followed in order to develop the coupled equations may differ from what is usually found in literature (which usually relies on the Helmholtz equation). If all these methods result in about the same analytical expression for the coupling constant Eq.(15) (assuming weak contrast, and identical waveguides), they rely on different approximations. Therefore it could also be interesting to assess how our approach may remain suitable for systems other than the one presented here. First, we demonstrate in Appendix D that Eq.(13) remains valid also for periodic waveguide, like for example Photonic Crystal waveguides. The matrix elements keep the same expression as defined in Eq.(12), the integral over the surface simply becoming an integral over the volume of the unit-cell. Note that considering the specific characteristic of the periodic systems, where the frequency $\omega$ is usually expressed as function of the wave-vector $\beta_b$, the formulation of the eigen-problem in term of $\omega$ rather than $\beta$ could be more appropriate.
Secondly, the derivation of any coupled modes equation involves a few assumptions at some point. In this regard we warn the reader to be cautious when applying ready-made formula, like Eq.(15), to other systems. In particular, the formula presented in this article assumes an hermitian evolution of a well defined, hence normalized, hence non-leaky, optical mode. Future work shall focus on leaky and non-hermitian systems. This is where numerous new applications and innovative strategies are developed; and therefore where having an analytical model to understand these systems could be of great interest. As a typical example, we discuss the strategy that consists in the use of gratings (hence leaky modes) as multiplexer to couple distant plasmonics (hence non-hermitian) waveguides [63]. If a complete case-study exceeds the scope of the present article, we can still provide some indications about how such a system must be taken into account by the coupled mode theory. The passage from Eq.(7) to Eq.(8) requires that $\left\langle \psi_0^{(i)} \right|$ is eigen-mode of $\hat{A}^*$. Therefore in case $\hat{A}$ is not hermitian, $\left\langle \psi_0^{(i)} \right|$ must be replaced by $\left\langle \psi_0^{(i)\dagger} \right|$, which is solution of the adjoint operator. Throughout this article, the operator $\hat{B}$ serves as normalization factor: it can be interpreted as a direct application of the Lorentz's reciprocity theorem. For leaky modes, likes found on gratings, modes are then Quasi Normal Modes [64], and the ortho-normalization procedure must then be changed accordingly [65, 66]. This usually consists using the non-conjugated form of the Lorentz reciprocity theorem.

## VIII. CONCLUSION

We demonstrated that the Local Field Effect (LFE) is an important feature in semiconductor integrated photonics, where contrast indices are large. We also showed the importance of the concept of the effective dielectric background $\varepsilon_{\mathrm{bg}}$ which is involved both in the description of the field decay and the LFE contribution. We hence managed to derive simple analytical formula an order of magnitude more accurate than previous developments found in literature. This study was also the occasion to draw the limits of this analytical approach to

describe coupled waveguides systems. These limitations are particularly stringent for high contrast ($\Delta\varepsilon > 1$) but low decay ($\sqrt{n_{\text{eff}}^2 - \varepsilon_{\text{bg}}} \leq 1$) systems, which include precisely a class of emerging materials (e.g. $TiO_2$, $Ta_2O_5$) for photonic integrated chips. If one can argue that with modern computing capability, the exact coupling constants can be computed in a timely manner, our study has nevertheless some profound implications. First it demonstrates the impact of the interplay between the cladding and the (structured) substrate on the optical mode properties. This reinforces our vision that a structured substrate forming a metamaterial [67] can be of great importance to tune further the optical properties of integrated photonic circuits. Secondly, if the current development would require some small adjustments of its parameters in order to match exactly the numerical simulation, it nevertheless takes into account the physics of the systems as precisely as possible. In particular the effective background provides the correct model for the decay of the coupling with increasing inter-waveguide separation. Moreover the chromatic dispersion due to the waveguide's geometry is also now much better described. Therefore it is possible to infer more precisely how the coupling features are a priori impacted by any change in the nominal parameters like, for instance, deriving the wavelength dependence of the coupling constant. The key advantage of the development that we propose here is that it allows to construct at minimal computational cost a test-function basis (or projection basis - Eq.(8)) as complete -or realistic- as possible. Such a strategy has been already permitted to accelerate RCWA algorithms [68]. Finally, by proving the suitability of the LFE concept even in the case of extended defects, this study is also of importance for, and can be extended to, any other systems requiring approximate solutions in photonics at minimal computation cost. Indeed the LFE allows a first estimation of the modification induced by a dielectric perturbation on the electric field. In particular optimization methods based on gradient computation [69] could greatly benefit from the LFE.

## ACKNOWLEDGMENTS

This work was supported by the Agence Nationale de la Recherche (ANR) project "NAC-NIP" (contract ANR-20-CE24-0007).

The authors declare no conflicts of interest.

## Appendix A: Previous works

The data in Fig.1 (c,d) labeled as "Previous works" can be separated to three methods: data obtained from a simplified approach Eq.(15) [18, 19]; perturbative method Eq.(10) with longitudinal field included [23]; perturbative method with $\boldsymbol{E}_x$ and $\boldsymbol{E}_y \rightarrow \frac{\boldsymbol{D}_y}{\boldsymbol{\varepsilon}}$ (black line, yellow diamonds and blue circles in Fig.A1, respectively) [24]. The presented methods result in approximately the same

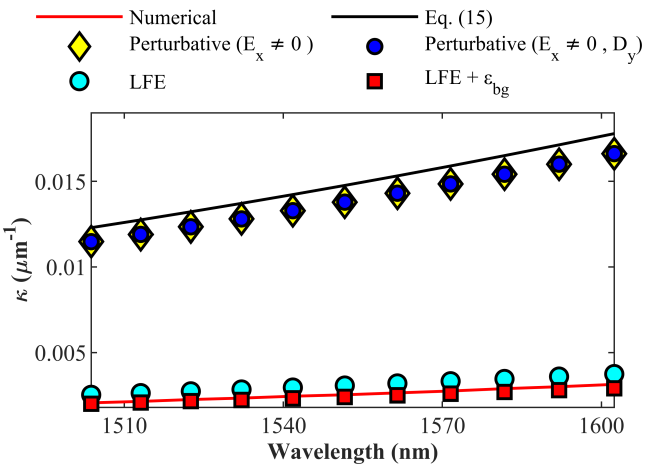


FIG. A1. Coupling constant $\kappa$ for two silicon waveguides separated by $G_1 = 220$ nm, as a function of the wavelength. Red line: numerical simulation. Black line: simplified analytical, from Eq.(15). Yellow diamonds: coupling constant resulting from the perturbative method (Eq.(10)) with longitudinal field $\boldsymbol{E}_x$ included. Dark blue circles: same as previous but continuity of $y$-field is preserved. Cyan circles: theory including the Local Field Effect (LFE). Red squares: theory including the LFE complemented by the concept of the effective background ($\varepsilon_{\text{bg}}$)

results; and they deviate substantially from the results of direct simulations.

## Appendix B: Simulation parameters (MPB)

Simulation are carried out using the MPB package [37]. For $Si$ waveguides we have used the following parameters : Global scaling factor of $a = 440\ nm$, Pixelsize 11 nm pixel$^{-1}$, Meshsize 12, Resolution 40, Tolerance $10^{-9}$, Range of eigenvalues $k = [0.57 : 1.1334]$ (normalized in $2\pi\ a^{-1}$ unit), Simulation geometry width = 24, height = 12 (in $a$-units).
For $SiN$ waveguides we have used the following parameters : Global scaling factor of $a = 650\ nm$, Pixelsize 65 nm pixel$^{-1}$, Meshsize 12, Resolution 40, Tolerance $10^{-9}$, Range of eigenvalues $k = [0.5871 : 0.8890]$ (normalized in $2\pi\ a^{-1}$ unit), Simulation geometry width = 18, height = 10 (in $a$-units).

Convergence is shown in Fig.B1 for the silicon waveguide (inter-waveguide spacing $G_1 = 330$ nm): the coupling coefficient $\kappa$ is computed with a relative precision of about 2.6%. The accuracy is absolute, so it impacts less the SiN waveguides which have strong evanescent field, and more situations with large inter-waveguide distance. In this regards, this shows that it is also equally important to have a reliable model to describe the evolution of the coupling constant with the inter-waveguide spac-

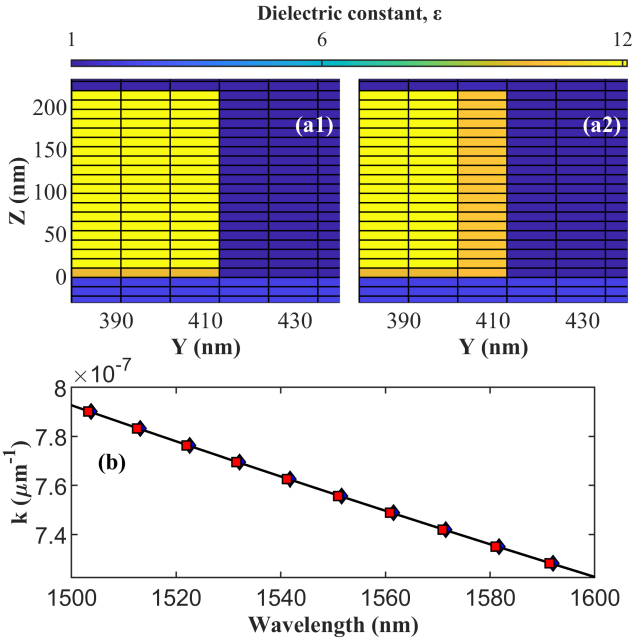


FIG. B1. (log-scale) Absolute error on the coupling constant $\kappa$, for silicon waveguides separated by $G_1 = 330\ nm$, depending on the grid resolution used for the simulation. Dark blue diamonds: situation when the grid in not properly aligned on the waveguides, which creates some smoothing of the dielectric interface. Red square : resolution chosen for this article (40 pixel $\mu m^{-1}$).

ing. Indeed weak coupling situations may not be computed accurately, or at huge computational cost. The simulation parameters and the waveguides' dimensions are selected to match exactly a discretization grid. Indeed, the MPB package assumes square pixels, therefore the features that do not match the grid exactly would be smoothed leading to a deviation from the assumed dielectric profile as shown on the blue diamonds in Fig.B1 where an increase of the inaccuracy by 25% is reported. These discrepancies will impact the eigenvalues and hence the accuracy regarding the coupling constant. To minimize the impact of the discretization, rectangular waveguides must be considered.

## Appendix C: LFE: case of homogeneous background

We present in Fig.C1 the analogue of Fig.2 in a case of an homogeneous air-cladding medium. This shows that when the cladding surrounding of the waveguide is composed of an uniform material, then $\varepsilon_{\text{bg}}$ indeed matches the nominal permittivity of the cladding.

## Appendix D: Periodic systems : Bloch-Floquet Modes Formulation

We show here that the formulas expressed in Eq.(13) and Eq.(14), and Eq.(15) remain valid for periodic waveguides subject that the integral over the surface being substituted by a volume integral over the single periodic cell.
The Bloch-Floquet theorem states that the a-periodic systems support eigen-modes that are a-periodic, to a phasor called the Bloch wave-vector; hence:

$$\begin{bmatrix} \boldsymbol{E}(x,y,z,t) \\ \boldsymbol{H}(x,y,z,t) \end{bmatrix} = \begin{bmatrix} \boldsymbol{u_E}(x,y,z) \\ \boldsymbol{u_H}(x,y,z) \end{bmatrix} e^{i\beta_b x - i\omega t} \tag{D1}$$

where $\boldsymbol{u_E}(x,y,z)$ and $\boldsymbol{u_H}(x,y,z)$ are a-periodic, hence $\boldsymbol{u}(x+a,y,z) = \boldsymbol{u}(x,y,z)$. As a consequence, the optical modes are not invariant by $\partial_x$ derivation.

$$\frac{\partial}{\partial x}|\psi\rangle = \imath\beta_b |\psi\rangle + \begin{bmatrix} \partial_x \boldsymbol{u_E}(x,y,z) \\ \partial_x \boldsymbol{u_H}(x,y,z) \end{bmatrix} e^{\imath\beta_b x - \imath\omega t} \tag{D2}$$

Let now compute the $\{i,j\}$ matrix elements associated to Eq.(3), corresponding to the equivalent of Eq.(8) for periodic structures.

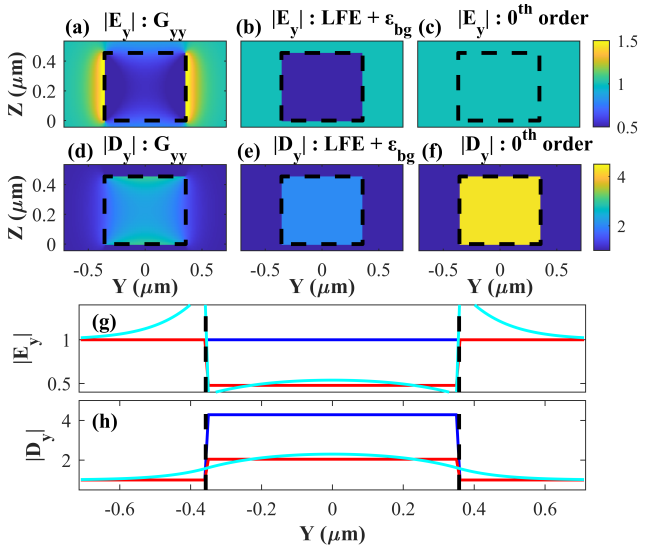


FIG. C1. Case of silicon nitride waveguides in air cladding, hence $\varepsilon_{\text{bg}} = 1$. (a-c) y-component of the Electric Field resulting from the perturbation of an initial homogeneous $E_y = 1$ field by a dielectric perturbation $\Delta\varepsilon$ which corresponds to the presence of the second waveguide. (a) is the solution of Eq.(16) restricted to the y-component of the field. (b) the result of the Local Field Effect assuming an effective background $\varepsilon_{\text{bg}} = \varepsilon_{\text{air}} = 1.00$. (c) Initial Coupled mode formulation where no changes of the Electric field are assumed (i.e. $0^{th}$ order theory). Black-dashed lines indicate the position of the dielectric perturbation and the limit with the air cladding. (d-f) y-component of the displacement field. (g-h) Variation of the electric Field (resp. Displacement Field) along y, for an altitude of 230 nm (Half the waveguide's height). Dark blue: zeroth order theory (no changes in the nominal electric field). Red: LFE theory assuming an effective background. Light Blue: Solution of Eq.(18).

$$\left\langle \psi_0^{(i)} \right| \frac{\partial}{\partial x} \hat{B} \left| \psi^{(j)} \right\rangle = \iint_S \left( \imath\beta_b \left[ \boldsymbol{u}_{\boldsymbol{E}}^{(\boldsymbol{i})*}, \boldsymbol{u}_{\boldsymbol{H}}^{(\boldsymbol{i})*} \right] \hat{B} \begin{bmatrix} \boldsymbol{u}_{\boldsymbol{E}}^{(\boldsymbol{j})} \\ \boldsymbol{u}_{\boldsymbol{H}}^{(\boldsymbol{j})} \end{bmatrix} + \left[ \boldsymbol{u}_{\boldsymbol{E}}^{(\boldsymbol{i})*}, \boldsymbol{u}_{\boldsymbol{H}}^{(\boldsymbol{i})*} \right] \hat{B} \begin{bmatrix} \boldsymbol{\partial_x} \boldsymbol{u}_{\boldsymbol{E}}^{(\boldsymbol{j})} \\ \boldsymbol{\partial_x} \boldsymbol{u}_{\boldsymbol{H}}^{(\boldsymbol{j})} \end{bmatrix} \right) e^{\imath(\beta_b - \beta_b^{(i)})x} \tag{D3}$$

$$\begin{aligned} \imath\frac{\omega}{c} \left\langle \psi_0^{(i)} \right| \hat{A} \left| \psi^{(j)} \right\rangle &= \imath\frac{\omega}{c} \iint_S \left[ \boldsymbol{u}_{\boldsymbol{E}}^{(\boldsymbol{i})*}, \boldsymbol{u}_{\boldsymbol{H}}^{(\boldsymbol{i})*} \right] \hat{A} \begin{bmatrix} \boldsymbol{u}_{\boldsymbol{E}}^{(\boldsymbol{j})} \\ \boldsymbol{u}_{\boldsymbol{H}}^{(\boldsymbol{j})} \end{bmatrix} e^{\imath(\beta_b - \beta_b^{(i)})x} \\ &= \imath\frac{\omega}{c} \iint_S \left( \left[ \boldsymbol{u}_{\boldsymbol{E}}^{(\boldsymbol{i})*}, \boldsymbol{u}_{\boldsymbol{H}}^{(\boldsymbol{i})*} \right] \hat{A}^{(i)} \begin{bmatrix} \boldsymbol{u}_{\boldsymbol{E}}^{(\boldsymbol{j})} \\ \boldsymbol{u}_{\boldsymbol{H}}^{(\boldsymbol{j})} \end{bmatrix} + \left[ \boldsymbol{u}_{\boldsymbol{E}}^{(\boldsymbol{i})*}, \boldsymbol{u}_{\boldsymbol{H}}^{(\boldsymbol{i})*} \right] \Delta\hat{A}^{(i)} \begin{bmatrix} \boldsymbol{u}_{\boldsymbol{E}}^{(\boldsymbol{j})} \\ \boldsymbol{u}_{\boldsymbol{H}}^{(\boldsymbol{j})} \end{bmatrix} \right) e^{\imath(\beta_b - \beta_b^{(i)})x} \end{aligned} \tag{D4}$$

$$\begin{aligned} &= \iint_S \left( \imath\beta_b^{(i)} \left[ \boldsymbol{u}_{\boldsymbol{E}}^{(\boldsymbol{i})*}, \boldsymbol{u}_{\boldsymbol{H}}^{(\boldsymbol{i})*} \right] \hat{B} \begin{bmatrix} \boldsymbol{u}_{\boldsymbol{E}}^{(\boldsymbol{j})} \\ \boldsymbol{u}_{\boldsymbol{H}}^{(\boldsymbol{j})} \end{bmatrix} - \left[ \partial_x \boldsymbol{u}_{\boldsymbol{E}}^{(\boldsymbol{i})*}, \partial_x \boldsymbol{u}_{\boldsymbol{H}}^{(\boldsymbol{i})*} \right] \hat{B} \begin{bmatrix} \boldsymbol{u}_{\boldsymbol{E}}^{(\boldsymbol{j})} \\ \boldsymbol{u}_{\boldsymbol{H}}^{(\boldsymbol{j})} \end{bmatrix} \right. \\ &\qquad \left. + \imath\frac{\omega}{c} \left[ \boldsymbol{u}_{\boldsymbol{E}}^{(\boldsymbol{i})*}, \boldsymbol{u}_{\boldsymbol{H}}^{(\boldsymbol{i})*} \right] \Delta\hat{A}^{(i)*} \begin{bmatrix} \boldsymbol{u}_{\boldsymbol{E}}^{(\boldsymbol{j})} \\ \boldsymbol{u}_{\boldsymbol{H}}^{(\boldsymbol{j})} \end{bmatrix} \right) e^{\imath(\beta_b - \beta_b^{(i)})x} \end{aligned} \tag{D5}$$

The Operator $\hat{A}$ has been decomposed into $\hat{A} = \hat{A}^{(i)} + \Delta\hat{A}^{(i)}$. Transforming Eq.(D4) into Eq.(D5) relies on the fact that $\left|\psi^{(i)}\right\rangle$ is solution of the adjoint equation to Eq.(3), hence:

$$\frac{\partial}{\partial x} \hat{B} \left| \psi \right\rangle = \imath\frac{\omega}{c} \hat{A}^{(i)*} \left| \psi \right\rangle \tag{D6}$$

The periodic nature of $\boldsymbol{u}$ can be put to use by integrating Eq.(D4) and Eq.(D5) along $\boldsymbol{x}$ over a periodic unit-cell. In such case, we have indeed the identity:

$$\int_{x=0}^{a}\left[\partial_x \boldsymbol{u}_{\boldsymbol{E}}^{(i)*},\partial_x \boldsymbol{u}_{\boldsymbol{H}}^{(i)*}\right]\hat{B}\begin{bmatrix}\boldsymbol{u}_{\boldsymbol{E}}^{(j)}\\ \boldsymbol{u}_{\boldsymbol{H}}^{(j)}\end{bmatrix} = \left[\left[\boldsymbol{u}_{\boldsymbol{E}}^{(i)*},\boldsymbol{u}_{\boldsymbol{H}}^{(i)*}\right]\hat{B}\begin{bmatrix}\boldsymbol{u}_{\boldsymbol{E}}^{(j)}\\ \boldsymbol{u}_{\boldsymbol{H}}^{(j)}\end{bmatrix}\right]_{x=0}^{a} - \int_{x=0}^{a}\left[\boldsymbol{u}_{\boldsymbol{E}}^{(i)*},\boldsymbol{u}_{\boldsymbol{H}}^{(i)*}\right]\hat{B}\begin{bmatrix}\boldsymbol{\partial_x} \boldsymbol{u}_{\boldsymbol{E}}^{(j)}\\ \boldsymbol{\partial_x} \boldsymbol{u}_{\boldsymbol{H}}^{(j)}\end{bmatrix}$$
$$= -\int_{x=0}^{a}\left[\boldsymbol{u}_{\boldsymbol{E}}^{(i)*},\boldsymbol{u}_{\boldsymbol{H}}^{(i)*}\right]\hat{B}\begin{bmatrix}\boldsymbol{\partial_x} \boldsymbol{u}_{\boldsymbol{E}}^{(j)}\\ \boldsymbol{\partial_x} \boldsymbol{u}_{\boldsymbol{H}}^{(j)}\end{bmatrix} \tag{D7}$$

Dropping the common phasor term $\exp \imath(\beta_b - \beta_b^{(i)})x$ in Eq.(D3) and Eq.(D5), and integrating these two equation over a unit-cell along $\boldsymbol{x}$ results finally after some simplifications in:

$$\imath\beta_b \iiint_V \left[\boldsymbol{u}_{\boldsymbol{E}}^{(i)*},\boldsymbol{u}_{\boldsymbol{H}}^{(i)*}\right]\hat{B}\begin{bmatrix}\boldsymbol{u}_{\boldsymbol{E}}^{(j)}\\ \boldsymbol{u}_{\boldsymbol{H}}^{(j)}\end{bmatrix} = \imath\beta_b^{(i)} \iiint_V \left[\boldsymbol{u}_{\boldsymbol{E}}^{(i)*},\boldsymbol{u}_{\boldsymbol{H}}^{(i)*}\right]\hat{B}\begin{bmatrix}\boldsymbol{u}_{\boldsymbol{E}}^{(j)}\\ \boldsymbol{u}_{\boldsymbol{H}}^{(j)}\end{bmatrix} + \imath\frac{\omega}{c}\left[\boldsymbol{u}_{\boldsymbol{E}}^{(i)*},\boldsymbol{u}_{\boldsymbol{H}}^{(i)*}\right]\Delta\hat{A^{(i)*}}\begin{bmatrix}\boldsymbol{u}_{\boldsymbol{E}}^{(j)}\\ \boldsymbol{u}_{\boldsymbol{H}}^{(j)}\end{bmatrix} \tag{D8}$$

Consequently, if we redefine the scalar product between two term as the integral over the unit-cell of their respective periodic parts (hence $\{\boldsymbol{u_E}, \boldsymbol{u_H}\}$ instead of $\{\boldsymbol{E}, \boldsymbol{H}\}$), Eq.(D8) can be re-written as :

$$\left(\beta_b - \beta_b^{(i)}\right)\left\langle \psi_0^{(i)}\right| \hat{B}\left|\psi^{(j)}\right\rangle = \frac{\omega}{c}\left\langle \psi_0^{(i)}\right| \Delta\hat{A^{(i)}}\left|\psi^{(j)}\right\rangle \tag{D9}$$

Which is exactly the matrix elements associated to Eq.(8). If the Bloch-Floquet modes are not strictly eigen-solutions of the Eq.(3), the perturbative problem can still be put into a set of equations that has exactly the same formulation as Eq.(13).

* Corresponding author: pierre.colman@u-bourgogne.fr


[1] N. C. Harris, J. Carolan, D. Bunandar, M. Prabhu, M. Hochberg, T. Baehr-Jones, M. L. Fanto, A. M. Smith, C. C. Tison, P. M. Alsing, and D. Englund, Linear programmable nanophotonic processors, Optica **5**, 1623 (2018).

[2] X. Yi, T. X. H. Huang, and R. Minasian, Tunable and reconfigurable photonic signal processor with programmable all-optical complex coefficients, Microwave Theory and Techniques, IEEE Transactions on **58**, 3088 (2010).

[3] W.-P. Huang, Coupled-mode theory for optical waveguides: an overview, J. Opt. Soc. Am. A **11**, 963 (1994).

[4] A. Yulin, D. V. Skryabin, and A. Vladimirov, Modulational instability of discrete solitons in coupled waveguides with group velocity dispersion, Optics Express **14**, 12347 (2006).

[5] I. Babushkin, A. Husakou, J. Herrmann, and Y. S. Kivshar, Frequency-selective self-trapping and supercontinuum generation in arrays of coupled nonlinear waveguides, Optics Express **15**, 11978 (2007).

[6] A. Joushaghani, R. Iyer, J. K. S. Poon, J. S. Aitchison, C. M. de Sterke, J. Wan, and M. M. Dignam, Quasi-bloch oscillations in curved coupled optical waveguides, Physical Review Letters **103**, 143903 (2009).

[7] Y. Lahini, E. Frumker, Y. Silberberg, S. Droulias, K. Hizanidis, R. Morandotti, and D. N. Christodoulides, Discrete x-wave formation in nonlinear waveguide arrays, Physical Review Letters **98**, 023901 (2007).

[8] S. Longhi, Quantum-optical analogies using photonic structures, Laser & Photonics Reviews **3**, 243 (2009), https://onlinelibrary.wiley.com/doi/pdf/10.1002/lpor.200810055.

[9] S. Longhi, M. Marangoni, M. Lobino, R. Ramponi, P. Laporta, E. Cianci, and V. Foglietti, Observation of dynamic localization in periodically curved waveguide arrays, Physical Review Letters **96**, 243901 (2006).

[10] G. Lenz, I. Talanina, and C. M. de Sterke, Bloch oscillations in an array of curved optical waveguides, Physical Review Letters **83**, 963 (1999).

[11] N. Chiodo, G. D. Valle, R. Osellame, S. Longhi, G. Cerullo, R. Ramponi, P. Laporta, and U. Morgner, Imaging of bloch oscillations in erbium-doped curved waveguide arrays, Optics Letters **31**, 1651 (2006).

[12] R. El-Ganainy, K. G. Makris, D. N. Christodoulides, and Z. H. Musslimani, Theory of coupled optical PT-symmetric structures, Optics Letters **32**, 2632 (2007).

[13] N. K. Efremidis, Topological photonic su-schrieffer-heeger-type coupler, Physical Review A **104**, 053531 (2021).

[14] N. Malkova, I. Hromada, X. Wang, G. Bryant, and Z. Chen, Observation of optical shockley-like surface states in photonic superlattices, Optics Letters **34**, 1633 (2009).

[15] J. T. Young, C. Wei, C. R. Menyuk, and J. Hu, Mode coupling at avoided crossings in slab waveguides with comparison to optical fibers: tutorial, Journal of the Optical Society of America B **38**, F104 (2021).

[16] Y. Liu, C. Wu, X. Qiang, J. Wu, X. Yang, and P. Xu, Evanescent-wave coupling phase-matching for ultrawidely tunable frequency conversion in silicon-waveguide chips, Optics Express **27**, 28866 (2019).

[17] B. Liu, H. Yu, Z. yuan Li, and L. Tong, Phase-matched second-harmonic generation in coupled nonlinear optical waveguides, Journal of the Optical Society of America B **36**, 2650 (2019).

[18] A. Hardy and W. Streifer, Coupled mode theory of parallel waveguides, Journal of Lightwave Technology **3**, 1135 (1985).

[19] H. Haus, W. Huang, S. Kawakami, and N. Whitaker, Coupled-mode theory of optical waveguides, Journal of Lightwave Technology **5**, 16 (1987).

[20] J. Ding, J. Lin, and Y. Sun, Calculation of coupling length for spatial waveguides using planar waveguides, Optik **126**, 4319 (2015-12).

[21] M. Kuznetsov, Expressions for the coupling coefficient of a rectangular-waveguide directional coupler, Optics Letters **8**, 499 (1983).

[22] S. Kim, K. Han, C. Wang, J. A. Jaramillo-Villegas, X. Xue, C. Bao, Y. Xuan, D. E. Leaird, A. M. Weiner, and M. Qi, Dispersion engineering and frequency comb generation in thin silicon nitride concentric microresonators, Nature Communications **8**, 10.1038/s41467-017-00491-x (2017).

[23] N. Kohli, S. Srivastava, and E. K. Sharma, Orthogonal solutions for asymmetric strongly coupled waveguide arrays: an elegant, analytical approach, Journal of the Optical Society of America B **31**, 2871 (2014).

[24] S. G. Johnson, M. Ibanescu, M. A. Skorobogatiy, O. Weisberg, J. D. Joannopoulos, and Y. Fink, Perturbation theory for maxwell's equations with shifting material boundaries, Physical Review E **65**, 066611 (2002).

[25] M. Skorobogatiy, M. Ibanescu, S. G. Johnson, O. Weisberg, T. D. Engeness, M. Soljačić, S. A. Jacobs, and Y. Fink, Analysis of general geometric scaling perturbations in a transmitting waveguide: fundamental connection between polarization-mode dispersion and group-velocity dispersion, Journal of the Optical Society of America A **19**, 2867 (2002).

[26] M. Skorobogatiy, S. Jacobs, S. Johnson, and Y. Fink, Geometric variations in high index-contrast waveguides, coupled mode theory in curvilinear coordinates, Optics Express **10**, 1227 (2002).

[27] E. Marcatili, Improved coupled-mode equations for dielectric guides, IEEE Journal of Quantum Electronics **22**, 988 (1986).

[28] S. Ghadirli, K. Thyagarajan, and A. Kumar, Band stop filter characteristics of non identical waveguides directional couplers; a comparison of three methods, Optics Communications **84**, 144 (1991).

[29] K. Okamoto, Coupled mode theory, in *Fundamentals of Optical Waveguides* (Elsevier, 2006) pp. 159–207.

[30] P.-R. Loh, A. F. Oskooi, M. Ibanescu, M. Skorobogatiy, and S. G. Johnson, Fundamental relation between phase and group velocity, and application to the failure of perfectly matched layers in backward-wave structures, Physical Review E **79**, 065601(R) (2009).

[31] X. C. Tong, Silicon-on-insulator waveguides, in *Advanced Materials for Integrated Optical Waveguides* (Springer International Publishing, 2013) pp. 253–287.

[32] H. Yıldırım, Dispersion parameters and nonlinear optical properties of silicon nitride rib waveguides, Optics Communications **284**, 2031 (2011).

[33] J. Wang, Z. Yao, and A. W. Poon, Silicon-nitride-based integrated optofluidic biochemical sensors using a coupled-resonator optical waveguide, Frontiers in Materials **2**, 10.3389/fmats.2015.00034 (2015).

[34] K. Hammani, L. Markey, M. Lamy, B. Kibler, J. Arocas, J. Fatome, A. Dereux, J.-C. Weeber, and C. Finot, Octave spanning supercontinuum in titanium dioxide waveguides, Applied Sciences **8**, 543 (2018).

[35] J.-C. Weeber, K. Hammani, G. C. des Francs, A. Bouhelier, J. Arocas, A. Kumar, F. Eloi, S. Buil, X. Quélin, J.-P. Hermier, M. Nasilowski, and B. Dubertret, Colloidal quantum dot integrated light sources for plasmon mediated photonic waveguide excitation, ACS Photonics **3**, 844 (2016).

[36] M. Belt, M. L. Davenport, J. E. Bowers, and D. J. Blumenthal, Ultra-low-loss ta_2o_5-core/SiO_2-clad planar waveguides on si substrates, Optica **4**, 532 (2017).

[37] S. G. Johnson and J. D. Joannopoulos, Block-iterative frequency-domain methods for maxwell's equations in a planewave basis, Opt. Express **8**, 173 (2001).

[38] A. W. Snyder and J. D. Love, Green's function methods, in *Optical Waveguide Theory* (Springer US, 1983) pp. 656–665.

[39] L. Ramunno and S. Hughes, Disorder-induced resonance shifts in high-index-contrast photonic crystal nanocavities, Physical Review B **79**, 161303(R) (2009).

[40] A. Yaghjian, Electric dyadic green's functions in the source region, Proceedings of the IEEE **68**, 248 (1980).

[41] O. J. F. Martin and N. B. Piller, Electromagnetic scattering in polarizable backgrounds, Physical Review E **58**, 3909 (1998).

[42] S. G. Johnson, M. L. Povinelli, M. Soljačić, A. Karalis, S. Jacobs, and J. D. Joannopoulos, Roughness losses and volume-current methods in photonic-crystal waveguides, Applied Physics B **81**, 283 (2005).

[43] P. V. Rysselberghe, Remarks concerning the clausius-mossotti law, The Journal of Physical Chemistry **36**, 1152 (1932).

[44] C. Böttcher, *Theory of Electric Polarization* (Elsevier, 1973).

[45] V. A. Markel, Introduction to the maxwell garnett approximation: tutorial, Journal of the Optical Society of America A **33**, 1244 (2016).

[46] M. B. Doost, W. Langbein, and E. A. Muljarov, Resonant state expansion applied to two-dimensional open optical systems, Physical Review A **87**, 043827 (2013).

[47] S. V. Lobanov, W. Langbein, and E. A. Muljarov, Resonant-state expansion applied to three-dimensional open optical systems: Complete set of static modes, Physical Review A **100**, 063811 (2019).

[48] J. E. Sipe, Vector k-p approach for photonic band structures, Physical Review E **62**, 5672 (2000).

[49] P. Y. Chen, D. J. Bergman, and Y. Sivan, Generalizing normal mode expansion of electromagnetic green's tensor to open systems, Physical Review Applied **11**, 044018 (2019).

[50] S. Rao, G. L. Saux, Y. Sivan, and P. Y. Chen, Generalized normal mode expansion method for open and lossy periodic structures, Journal of the Optical Society of America B **39**, 1338 (2022).

[51] P. T. Kristensen, J. R. de Lasson, and N. Gregersen, Calculation, normalization, and perturbation of quasinormal modes in coupled cavity-waveguide systems, Optics Letters **39**, 6359 (2014).

[52] M. L. Cooper and S. Mookherjea, Numerically-assisted coupled-mode theory for silicon waveguide couplers and arrayed waveguides, Optics Express **17**, 1583 (2009).

[53] M. Patterson and S. Hughes, Interplay between disorder-induced scattering and local field effects in photonic crystal waveguides, Phys. Rev. B **81**, 245321 (2010).

[54] N. Mann, A. Javadi, P. D. García, P. Lodahl, and S. Hughes, Theory and experiments of disorder-induced resonance shifts and mode-edge broadening in deliberately disordered photonic crystal waveguides, Physical

Review A **92**, 023849 (2015).
[55] V. LeBihan, A. Pillonnet, D. Amans, G. Ledoux, O. Marty, and C. Dujardin, Critical dimension where the macroscopic definition of refractive index can be applied at a nanometric scale, **78**, 113405 (20008).
[56] P. Lunnemann and A. F. Koenderink, The local density of optical states of a metasurface, Scientific Reports **6**, 10.1038/srep20655 (2016).
[57] M. Patterson, S. Hughes, D. Dalacu, and R. L. Williams, Broadband purcell factor enhancements in photonic-crystal ridge waveguides, Phys. Rev. B **80**, 125307 (2009).
[58] M. Eguchi, Multilayered effective-index analysis of dielectric waveguides with complicated microstructures, Journal of the Optical Society of America B **28**, 2478 (2011).
[59] N. Mann, S. Combrié, P. Colman, M. Patterson, A. D. Rossi, and S. Hughes, Reducing disorder-induced losses for slow light photonic crystal waveguides through bloch mode engineering, Opt. Lett. **38**, 4244 (2013).
[60] K. S. Chiang, Performance of the effective-index method for the analysis of dielectric waveguides, Optics Letters **16**, 714 (1991).
[61] T. A. van der Sijs, O. ElGawhary, and H. P. Urbach, Electromagnetic scattering beyond the weak regime: Solving the problem of divergent born perturbation series by padé approximants, Physical Review Research **2**, 013308 (2020).
[62] O. J. F. Martin, A. Dereux, and C. Girard, Iterative scheme for computing exactly the total field propagating in dielectric structures of arbitrary shape, Journal of the Optical Society of America A **11**, 1073 (1994).
[63] A. Udupi and S. K. Madhava, Plasmonic coupler and multiplexer/demultiplexer based on nano-groove-arrays, Plasmonics **16**, 1685 (2021).
[64] P. Lalanne, C. Sauvan, J. P. Hugonin, J. C. Rodier, and P. Chavel, Perturbative approach for surface plasmon effects on flat interfaces periodically corrugated by subwavelength apertures, Physical Review B **68**, 125404 (2003).
[65] P. Lalanne, W. Yan, K. Vynck, C. Sauvan, and J.-P. Hugonin, Light interaction with photonic and plasmonic resonances, Laser and Photonics Reviews **12**, 1700113 (2018).
[66] C. Sauvan, J. P. Hugonin, I. S. Maksymov, and P. Lalanne, Theory of the spontaneous optical emission of nanosize photonic and plasmon resonators, Physical Review Letters **110**, 237401 (2013).
[67] M. B. Mia, S. Z. Ahmed, I. Ahmed, Y. J. Lee, M. Qi, and S. Kim, Exceptional coupling in photonic anisotropic metamaterials for extremely low waveguide crosstalk, Optica **7**, 881 (2020).
[68] L. C. Andreani and D. Gerace, Photonic-crystal slabs with a triangular lattice of triangular holes investigated using a guided-mode expansion method, Phys. Rev. B **73**, 235114 (2006).
[69] J. Jensen and O. Sigmund, Topology optimization for nano-photonics, Laser and Photonics Reviews **5**, 308 (2010).